AIAA 2013-2234

Toward Active Control of Noise from Hot Supersonic Jets

A. Sinha[1]*, R. H. Schlinker[2]†, J. S. Simonich[2]‡, R. A. Reba[2]§ and T. Colonius[1]¶
[1] *Department of Mechanical Engineering, California Institute of Technology, Pasadena, CA*
[2] *Thermal and Fluid Sciences Department, United Technologies Research Center, E. Hartford, CT*

We present diagnostic experiments and reduced-order models aimed at understanding and mitigating supersonic jet noise from coherent wavepackets in the turbulent shear layer, generally accepted to be the source of peak aft-angle mixing noise. The work builds on a successful Caltech/UTRC modeling approach that predicts the evolution of the wavepackets as instability waves of the turbulent mean flow, as well as the noise radiated from their near field. The models are experimentally assessed for unforced and forced supersonic isothermal and heated Mach 1.5 jets from ideal expansion nozzles. A spinning valve device is used to inject air near the nozzle lip at frequencies up to a Strouhal number of about 0.25. Results indicate a 2-3 dB benefit near peak frequencies of the spectrum and a 2 dB OASPL reduction at a mass flow percentage of 3.2. For the same injection plenum pressure, steady blowing yields more noise benefit than the unsteady actuation schemes explored until now. However, this may be explained by the slight decrease in injection velocity incurred in going from steady to unsteady operation. The reduced-order models, based on parabolized stability equations (PSE), are found to be in good agreement, in terms of envelope and phase, with those educed from the experimental data of the unforced jet. For the actuation schemes we have considered to date, the model and experimental data support a tentative explanation for the observed noise reduction in terms of attenuation of the wavepacket amplitudes by the thickened shear layer. Wavepackets induced by the harmonic component of the actuation are linearly superposed on those produced by broadband turbulence, without significant interaction, such that they lead to the addition of tones to the far-field noise that are counterproductive as far as noise reduction is concerned.

I. Introduction

Design requirements for tactical aircraft include low drag and weight and high specific thrust, which favor small exit areas and supersonic exhaust velocities that result in noise levels that pose health problems for aircraft carrier launch/recovery crews. Currently, passive methods to increase jet mixing and break up shock cells in the over-expanded flow are being considered to reduce noise levels by up to several dB. These include chevrons, nozzle redesign to achieve ideal expansion, and lobed nozzle inserts. Active, deployable approaches that could avoid performance penalties in mission-critical portions of the flight envelope are a desirable alternative. Recent research on active control has centered on fluidic/air injection at the nozzle lip,[1,2] fluidic lobes inside the diverging section of the nozzle,[3] and plasma actuation at the nozzle lip.[4]

Both steady and unsteady fluidic injection strategies have been investigated in past. In the steady scheme, streamwise vortices generated near the nozzle enhance the mixing in a manner similar to chevrons.[5] In comparison, recent explorations indicate that improvements in the noise benefit to mass input ratio may be achievable through optimized unsteady injection.[2] However, the precise mechanism of noise reduction has not been addressed as yet. Whereas steady active control provide this sole benefit, unsteady (or pulsed)

*Postdoctoral Scholar, AIAA Member
†Principal Engineer, AIAA Associate Fellow
‡Staff Research Engineer
§Principal Research Scientist, AIAA Member
¶Professor, AIAA Associate Fellow, Corresponding author: colonius@caltech.edu

Table 1. Jet operating conditions.

Case	Description	NPR	NTR	M_j	M_∞	T_j	Re_j	M_T
B118	Isothermal ideally-expanded	3.55	1.45	1.5	1.5	1.0	16.2×10^5	0.05
B122	Heated ideally-expanded	3.51	2.53	1.5	1.98	1.74	8.2×10^5	0.05

control has the additional potential ability to manipulate the turbulent noise sources on their own time scales, potentially resulting in larger noise reductions than can be achieved with passive devices.

This article presents results of a concerted experimental and theoretical approach to understand and reduce supersonic jet mixing noise. The experiments employ a suite of diagnostics to track wavepacket structures that are the dominant source of aft-angle (peak) noise radiation in supersonic, fully turbulent, perfectly-expanded jets.[6,7] We introduce an existing actuation system involving a pair of spinning valves that were originally developed for combustion instability control at United Technologies Research Center (UTRC).[8] Each valve consists of a high-pressure air supply to a rotating drum with holes around the circumference that periodically align with matching holes in the surrounding housing, which, in turn, are connected to injection ports at the nozzle exit. This provides significant momentum addition to the jet at relatively high frequencies. Shaping of the holes may be used to independently control the perturbation waveform. Steady injection is obtained by holding the drum fixed with its holes aligned with the housing ports. Results are presented for Mach 1.5 jets, and both isothermal and heated conditions are investigated.

The use of the existing injection system avoided the actuator development phase, and instead allowed focusing the study on the cause-effect link between the injection, the near-field instability/wavepacket evolution, and the far-field sound. So, for the first time, a direct measurement is made of the real-time acoustic response to forcing and its relation to relevant flow structures and their spatio-temporal evolution.

The theoretical aspect builds on recent success in development of a physics-based, reduced-order model that has demonstrated remarkable accuracy in predicting the dynamics of wavepackets in unforced jets.[9–11] In this paper we extend the model to consider both unforced and forced supersonic jets, and use it, together with experimental observations, to explore the mechanisms of noise generation and reduction by active control.

II. Experimental setup

A. Test facility

Experimental studies are conducted in the UTRC Acoustic Research Tunnel (ART).[12] Briefly, the test section is surrounded by a sealed chamber 16 ft. high, 18 ft. long (in the jet centerline direction) and 22 ft. wide, that is anechoic above 175 Hz. The jet is supplied with high pressure air from a compressor system capable of delivering 20 lb/sec of dry air continuously. Heating is provided by a liquid propane burner.

The thin-lipped converging-diverging nozzle used in the experiments has an exit diameter D of 50.8 mm (2 in.) and is designed for a jet exit Mach number M_j of 1.5. Two shock-free supersonic jet conditions are tested;[12] their parameters are tabulated in table 1. Specifically, we note the acoustic Mach number M_∞, the nozzle exit static temperature ratio (referenced to the ambient) T_j, the nozzle exit Reynolds number Re_j, and the tunnel Mach number M_T, apart from nozzle pressure ratio (NPR), nozzle temperature ratio (NTR), and M_j. For a fixed NTR, the precise NPR was chosen to minimize the noise at the sideline microphone. This serves as a check for shock-free conditions in lieu of the ideal-expansion relations which do not account for the finite boundary-layer thickness at the nozzle exit. The set-points B118 and B122 are from an earlier test matrix.[13] Most of the experimental results will be presented for the heated jet, and some comparisons will be made with the isothermal condition.

B. Spinning-valve actuator

The actuator used to force the jet is a spinning valve devised by UTRC and used previously for active combustion instability control[14] and jet-in-cross-flow control.[8,15,16] Air supply is provided to a plenum inside a rotating drum (which is connected to a motor spool) with 40 holes around the periphery. Concentric

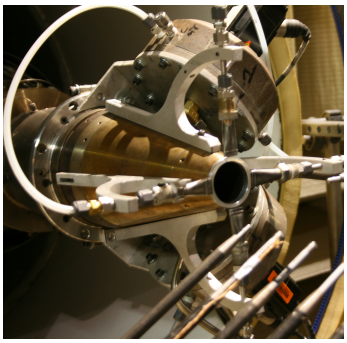

(a) Assembly of two actuators

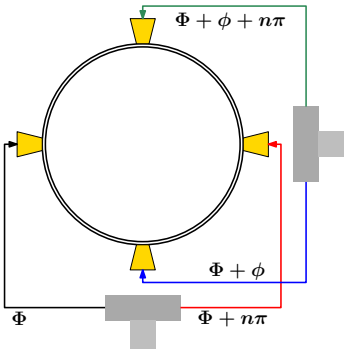

(b) Possible azimuthal forcing patterns

Figure 1. Features of the spinning valve actuator system.

to the rotating drum is an outer stationary cylinder, which has two diametrically opposed holes connected to injection ports. When the motor is operated at a fixed speed, air is delivered to the two outer (stationary) drum holes in a periodic (in-phase) fashion. An additional hole in the housing provides an optional 180° out-of-phase flow. When the motor used to actuate the valve is not operated but the shaft is fixed at a preset rotation angle, steady flow issues from the exit ports.

Air injection using the spinning valve is a useful choice of actuation since it provides significant momentum addition to the jet when compared to synthetic jets or plasma actuation. Unlike conventional reciprocating-spool configurations, the upper frequency limit of the spinning valve is not due to the spool inertia or power required to accelerate it. The upper speed range of the spinning valve used in the tests is 5000 RPM, but the motor is rated for 8000 RPM. The forcing frequency f_F is determined by the RPM and the hole count on the rotating drum. We report this in terms of the forcing Strouhal number $St_F := f_F D/U_j$, where U_j is the jet velocity at the nozzle exit.

Two such actuators with independent, but synchronizable, computer controlled servomotors are used to inject air into the shear layer of the jet normal to the centerline; the assembly is shown in figure 1(a). By suitably phasing the two motors (i.e. selecting ϕ in figure 1(b)) and choosing the housing holes to use (i.e. selecting the integer n in figure 1(b)), we can simulate perturbation at azimuthal modes $\mu = 0$, 1 and 2, as well as the first flapping mode. All results presented here are with $\mu = 0$. The injection ports have a 0.615 in. $\times$ 0.07 in. rectangular geometry with 0.05 in. thick walls.

C. Diagnostics

The mean flow field is probed using a total pressure pitot tube and total temperature thermocouple with a shielding and a bleed vent. The centerline of the jet is sampled at 25 points with logarithmic spacing in $0.25 \leq x/D \leq 30$. Radial profiles are sampled at 6 cross sections - viz. $x/D = 0.75$, 2.5, 4.5, 10, 15 and 20. Anticipating departures from axisymmetry in the forced conditions, radial surveys are conducted in two azimuthal planes – the first one passing through the center of one of the four injection ports (referred to as 0°), and the second one bisecting two ports (and hence at 45°). Each radial survey consists of 20 points spaced so as to adequately resolve the variations in the shear layer.

Jet hydrodynamic near-field pressure measurements are acquired using a rotating microphone array[17] shown in figure 2. This was specifically designed to identify the acoustically dominant wavepackets in the near irrotational pressure field, and to track their modification with variations in forcing parameters. The concept uses two linear arrays as depicted in figure 2(a). One array can be rotated on a motorized track in the azimuthal direction, while the second array (i.e. the reference array) is also movable, but requires manual adjustment. The array cage consists of two 51 in. diameter open rings and an open frame base to minimize acoustic reflections. For a given position of the reference array, phase-locked data are acquired on the two arrays for each unique azimuthal separation. Each linear array consists of 16 B&K type 4939 quarter-inch microphones, encompassing the first 20 jet diameters, as shown in figure 2(b). Microphone axial spacing ranges from $0.5D$ to $2.0D$, with larger spacing at the most down-stream locations. The spreading angle (cone half-angle) is 7°. Data is acquired at azimuthal increments of 15° over 210° of the azimuth.

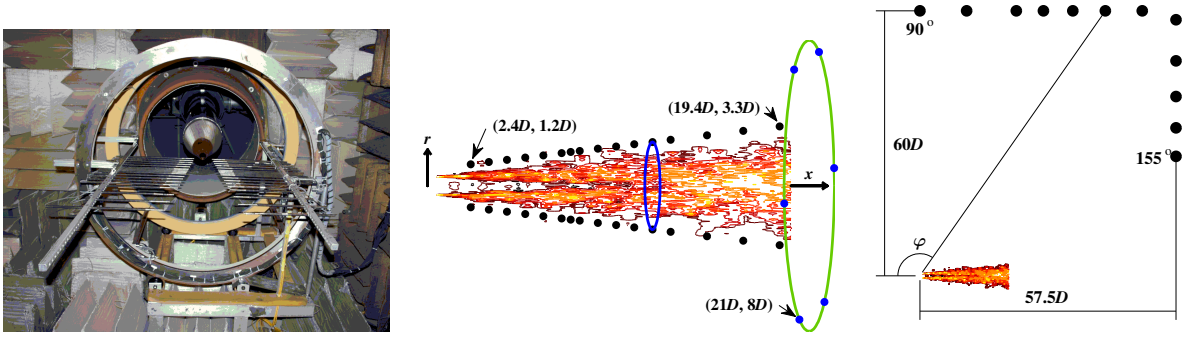

(a) Rotating near-field array (b) Layout of near and mid-field arrays (c) Layout of far-field polar array

Figure 2. Measurement setup for near-field pressure, and mid-field and far-field acoustics.

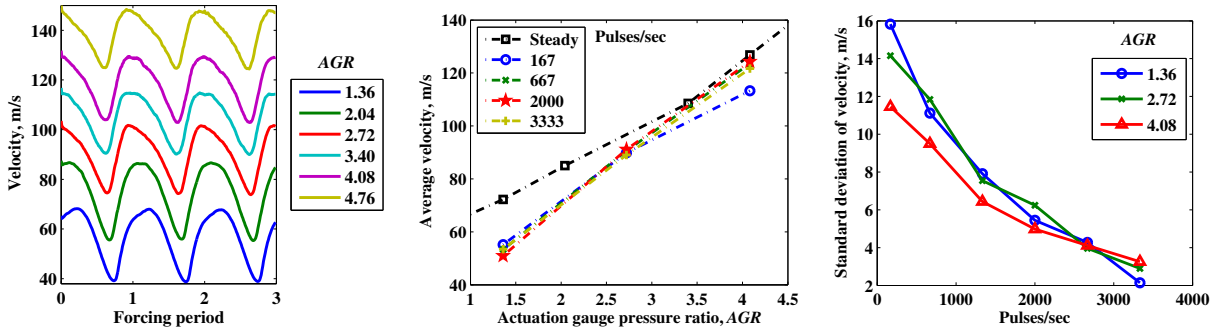

(a) Waveform at 667 pulses/sec (b) Mean component (c) Fluctuating component

Figure 3. Characterization of spinning valve actuation system with phase-averaging of injection velocity.

A uniform azimuthal array of 6 microphones is situated in the intermediate acoustic field, as shown in figure 2(b). They are at a polar angle of 159° from the upstream jet axis, and a polar radius of $22.5D$.

The far acoustic field is acquired using the 12 microphone stations schematically depicted in figure 2(c). The measurements encompass polar angles from 90° to 155° relative to the upstream jet axis at polar radii of $60D$ to $80D$ from the center of the nozzle exit.

All 50 microphone signals are simultaneously sampled using a DataMax DTX-9R data acquisition system at a 200 kHz sampling rate. Additionally, individual encoder signals from the two spinning valve controllers are also recorded on the same time base for phase-locked post-processing.

III. Actuator characterization

The actuator supply gauge pressure ratio (AGR) denotes the imposed upstream gauge pressure normalized by the ambient. No effort was made to optimize the actuation system within the present campaign and large pressure losses were incurred. For example, with the maximum imposed AGR of 5.4, the static pressure ratio at the port exit was about 0.2. Thus, the reported AGR values should be used merely to identify experimental set-points. The results presented here are mostly using the AGR of 5.4, and for steady blowing, the corresponding mass flow rate of injection was measured with a flow-meter as 32 g/s (from the two valves together). This translates to a mass flow percentage (MFP) with respect to the primary jet of 2.5% and 3.2% in the isothermal and heated jet, respectively. Results are also discussed for an AGR of 2.7, and the corresponding MFP are 1.6% and 2.0% for the two jets, respectively.

Hot-wire anemometry was used to record the centerline velocity at the injection port exit. Figure 3 characterizes the imposed harmonic forcing with the phase-averaged velocity. Owing to latencies in the piping downstream of the valve, the waveform departs from a rectangular shape. Moreover, it is observed that, the average injection velocity is a weak function of the pulse frequency, although there is a slight

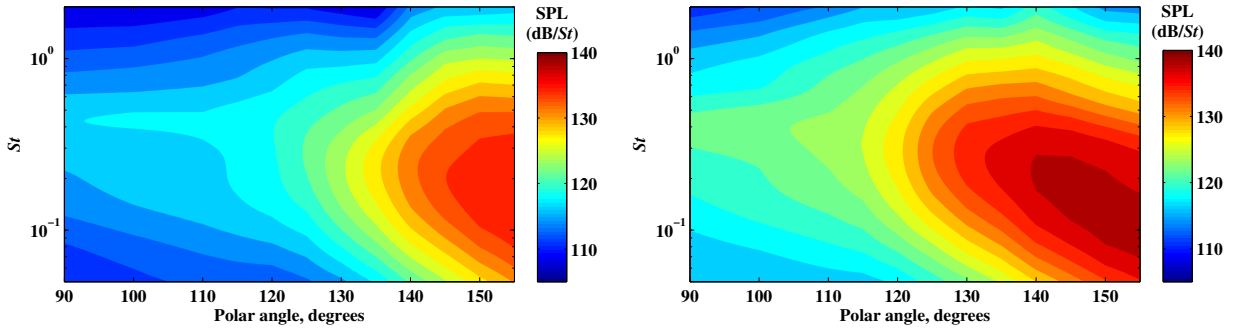

(a) Isothermal jet

(b) Heated jet

Figure 4. Spectral directivity of SPL in the unforced isothermal and heated jets.

decrease in going from steady to unsteady operation. The peak-to-peak amplitude of the injection velocity is characterized by the standard deviation of the phase-averaged waveform. It decreases monotonically with increasing pulse frequency, but appears to be relatively independent of the AGR. This further implicates latencies in the downstream piping of the actuation system, which could be improved in future versions of the actuation design.

IV. Experimental results

A. The noise benefit

Far-field acoustic measurements were acquired over a significant portion of the aft polar arc, and figure 4 shows the sound pressure level (SPL) at these microphones for the two unforced jets. The frequency f is reported as the non-dimensional Strouhal number $St = fD/U_j$, and the SPL is the power spectral density in dB per unit St, relative to 20×10^{-6} Pa. This figure illustrates several standard observations in jet noise studies – the noise generally peaks at aft angles, the spectral peak shifts to lower frequencies toward further aft angles, the spectra become flatter at the sideline angles, increasing the exit velocity (associated with heating the jet while holding the exit Mach number constant) increases the SPL and shifts the directivity peak toward sideline angles, and heating the jet shifts the spectral peak to lower Strouhal numbers. Given the orders-of-magnitude difference in noise levels between aft and sideline angles, noise modifications through flow control at sideline angles, if any, will have negligible impact on the perceived noise levels. In other words, noise changes that are equivalent in the dB scale are not equivalent in their practical impact. Thus, the detailed studies hereafter will focus on the 150° aft angle.

The forcing parameter space of the present actuators is large. Thus, the discussion is mainly restricted to cases where the actuators were supplied at the maximum AGR of 5.4, as discussed in § III. Only the axisymmetric mode of actuation is considered; i.e., the four ports are operated in phase. Finally, apart from the steady blowing condition, only a few representative forcing frequencies are discussed.

The SPL measured at the peak radiation polar angle of 150° are presented for the heated jet in figure 5(a) for three forcing Strouhal numbers along with the steady blowing case, all using an AGR of 5.4. Apart from the narrow-band forcing tones and their harmonics, reduction is observed over the entire spectral range. This is also confirmed in the delta values plotted in figure 5(c). (The forcing tones are removed for ease of visualization, but only for the ΔSPL plots in figures 5(d) and 5(c).) Peak reductions of around 3 dB are obtained at $St \sim 0.25$, which is past the spectral peak at $St \sim 0.1$. The steady blowing condition is slightly more effective than the pulsed cases. It was remarked in § III that, with the same AGR, the mean velocity at the injection port exit decreases slightly when going from steady to unsteady blowing. This may account for the corresponding decrease in noise benefits observed at higher forcing frequencies.

A similar scheme is followed in presenting the data over the entire polar arc in figures 5(e) and 5(g). Actuation is seen to increase the OASPL by about 1.5 dB at 120°. However, OASPL mitigation of about 2 dB is obtained in the peak noise radiation direction. Recalling the arguments presented in discussing figure 4, the latter noise benefit at the noisier angles is far more important than the amplification at the quieter angles. The dependency on the forcing frequency is weak.

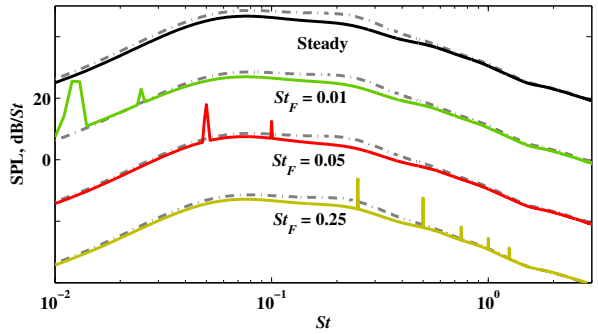

(a) SPL at 150° in the heated jet (– · – unforced)

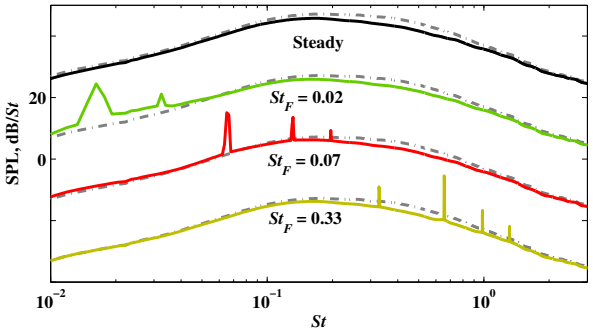

(b) SPL at 150° in the isothermal jet (– · – unforced)

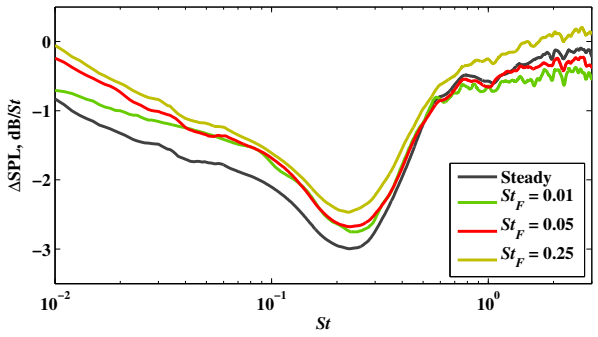

(c) ΔSPL at 150° in the heated jet (de-toned for clarity)

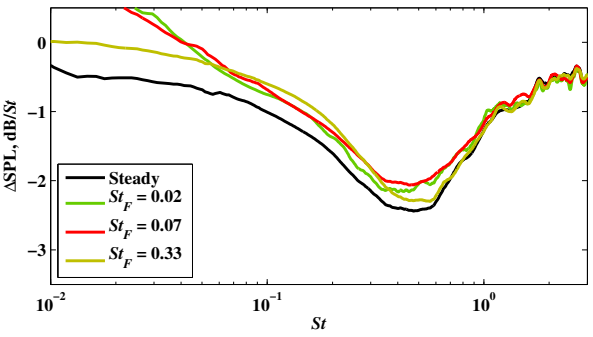

(d) ΔSPL at 150° in the isothermal jet (de-toned for clarity)

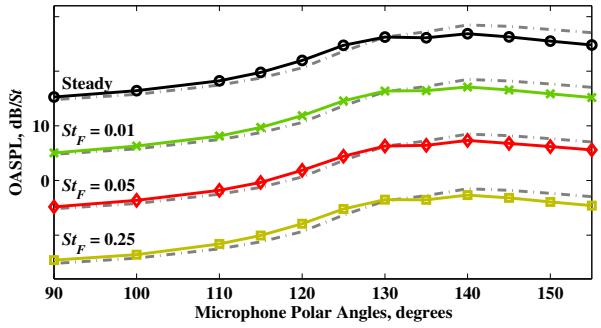

(e) OASPL in the heated jet (– · – unforced)

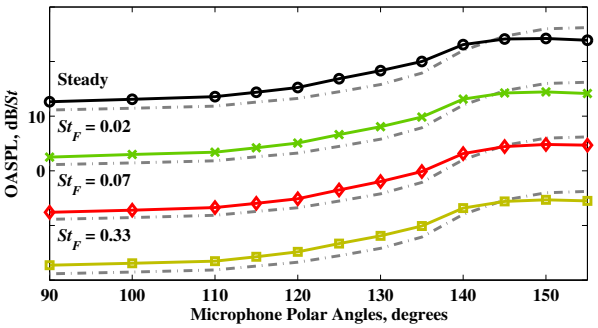

(f) OASPL in the isothermal jet (– · – unforced)

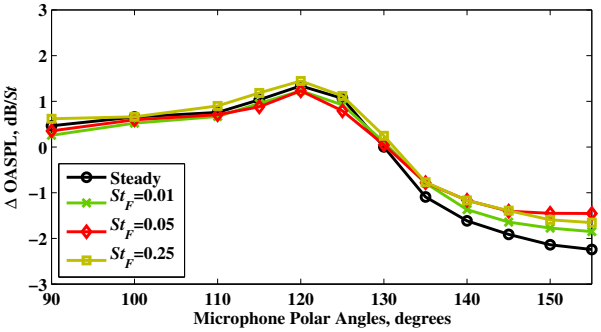

(g) ΔOASPL in the heated jet, with tones retained

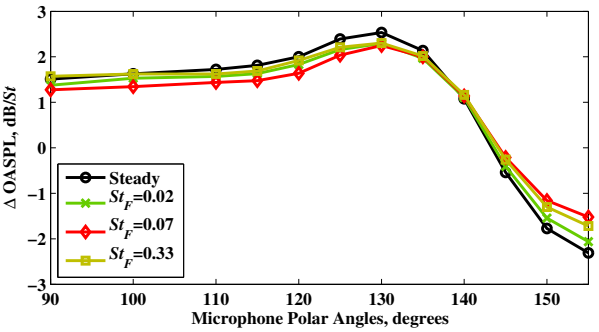

(h) ΔOASPL in the isothermal jet, with tones retained

Figure 5. Effect of different forcing parameters on the far-field noise in the (left) heated and (right) isothermal supersonic jets. The actuator supply gauge pressure ratio is 5.4 in all forced cases.

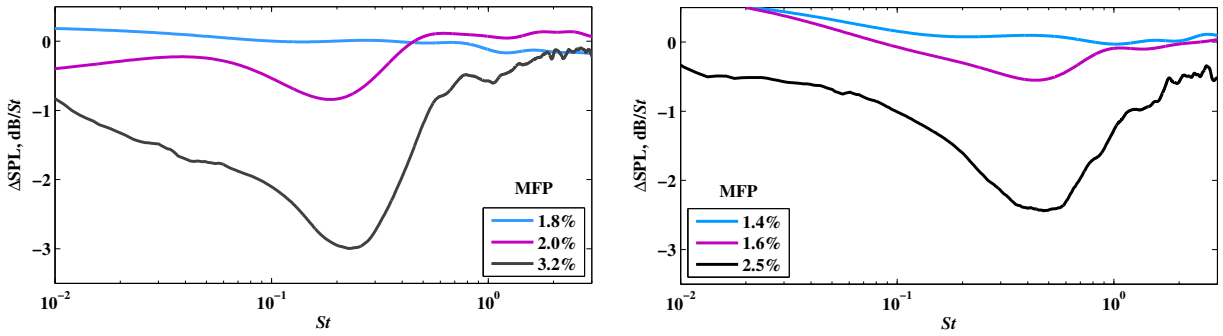

(a) Heated jet (b) Isothermal jet

Figure 6. Effect of mass flow percentage of steady blowing on the ΔSPL at the 150° microphone.

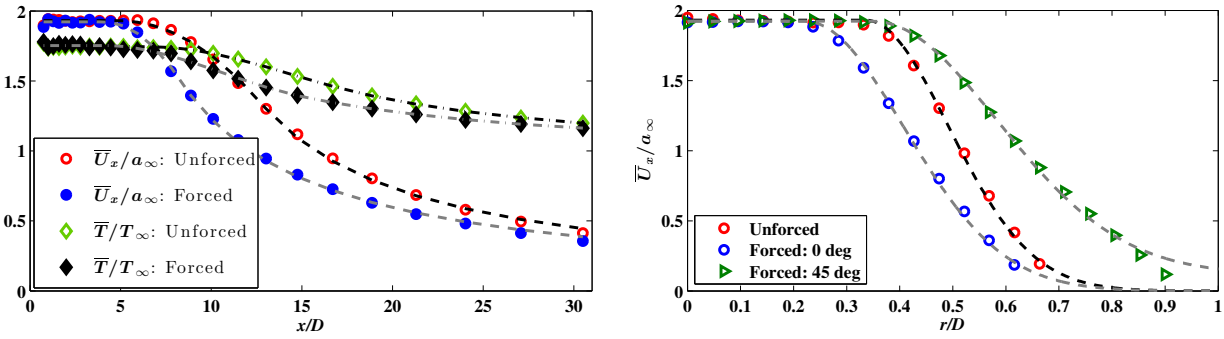

(a) Mean centerline velocity and temperature (b) Mean streamwise velocity profiles at $x/D = 3$

Figure 7. Effect of steady blowing at 3.2% mass flow on the mean flow field of the heated jet. The azimuthal plane through a port is indicated by '0 deg', and '45 deg' implies the plane bisecting two ports.

Representative results for the isothermal jet are also presented in figure 5 using a similar scheme. The peak reduction of 2.2 dB in ΔSPL measured at the 150° polar position is observed at a higher St of 0.5 with steady blowing. Pulsed blowing appears slightly less effective, although the trends are similar. In the ΔOASPL plots presented in figure 5(h), one observes some differences compared with the heated case. Over most of the polar arc, the noise reduction is slightly degraded in the isothermal jet. Although the peak OASPL reduction continues to be about 2 dB at the noisiest radiation angle, the drop-off of benefit at nearby angles is sharper in the isothermal jet. Moreover, the maximum amplification is about 2.5 dB now at 130°, and at least 1.5 dB over all sideline angles upstream of this.

Overall, it can be said that the actuators have increased control authority in the heated jet for the same injection mass flow rate. This may be an artifact of the increased mass flow percentage for the heated jet – the primary jet mass flow rate is inversely proportional to the square root of the stagnation temperature for constant jet exit Mach number.

For the sake of completeness, figure 6 presents the changes in the SPL at the 150° far-field microphone as a function of the mass flow percentage of steady blowing. For both the isothermal and heated jets, diminution of noise benefit at the lower injection rates explored is evident.

The suite of diagnostics deployed in the present experiments was designed to study jet noise from its source to the far field. In the following sections, we analyze these measurements to understand the physics behind the noise benefits reported above.

B. The mean flow field

Actuation substantially changes the mean flow field. Figure 7(a) shows that the potential core is shortened by steady blowing at the MFP of 3.2 on the heated jet. Defining the end of the potential core as the axial

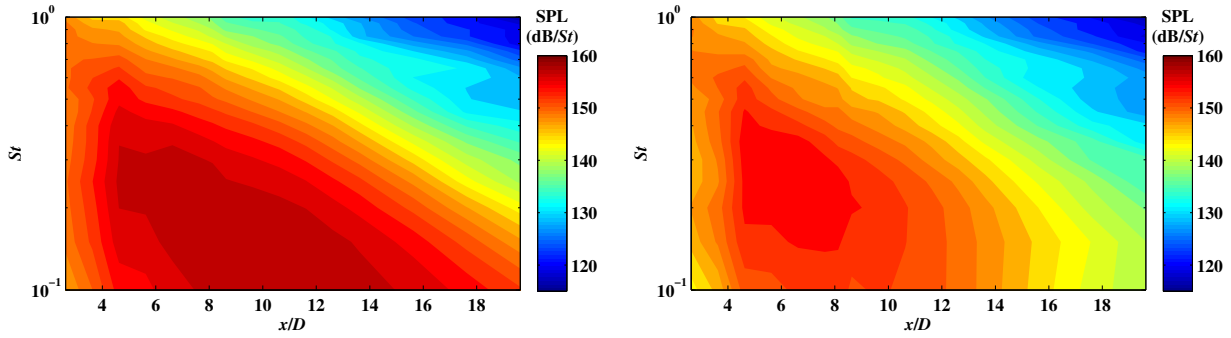

(a) Azimuthal mode $m = 0$ (b) Azimuthal mode $m = 1$

Figure 8. Power spectra on the near irrotational field microphone array in azimuthal modes 0 and 1 for the unforced heated jet.

station where the centerline velocity falls below 99% of the exit velocity, the forcing changes the length of the potential core from $6.3D$ to $4.8D$. Moreover, the initial rate of decay of the centerline velocity is higher as a result of forcing. Similar modifications are observed in the centerline temperature. Dramatic changes are also observed in the radial profiles at $x/D = 3$ in figure 7(b). In the azimuthal plane of an injection port, the shear layer is squeezed toward the centerline. In between two ports, the shear layer bulges out substantially. Moreover, the shear layer is thickened in both the azimuthal planes. Although not shown here, these changes in the radial profiles are insignificant beyond $x/D = 10$. These modifications to the mean flow field are similar to those produced by steady microjets observed by Alkislar et al.,[5] who attributed the changes to the development of streamwise vortices, similar to those produced by chevrons.

The velocity gradient in the shear layer determines the strength of the Kelvin-Helmholtz instability, which, in turn, has been shown to account for the growth and evolution of the acoustically dominant wavepackets.[7] Thus, the thickening of the shear layer with forcing anticipates the noise mitigation reported in § IV-A. This idea will be explored further with the reduced-order model in § V.

The model for wavepackets requires the mean jet velocity profile as the sole input. With the relatively sparse Pitot probe and thermocouple surveys, we attempt to fit several empirical functions to the data to obtain smooth fields. The details are provided in Appendix A, and the resulting empirical mean flow profiles are compared to the data in figure 7.

C. The near-field pressure

The lowest azimuthal Fourier modes, denoted by m, dominate the near-field pressure,[18,19] and the rotating cage array was designed to measure them. Indeed, over the range $0.05 \leq St \leq 0.5$ spanning the spectral peak, the $m = 2$ mode has 5 to 15 dB less energy than either the $m = 0$ or $m = 1$ modes (integrated over the length of the array). In these azimuthal modes, the preponderance of low-frequency fluctuations in the unforced heated jet is demonstrated in figure 8. This justifies the restriction of attention and subsequent reduced-order modeling effort to these Fourier mode pairs. This figure also demonstrates the shift of the spectral peak to lower frequencies as the observer moves downstream. The spectra peak at slightly higher frequencies in the $m = 1$ mode. At no axial station or frequency does the first helical mode supersede the axisymmetric mode. These characteristics were observed for the isothermal supersonic jet also. Here, and subsequently, the $m = 1$ mode energy is *not* doubled to add together the energy in $m = -1$ mode.

The amplitude comparisons are made on a linear scale instead of the log-scale used above. In dimensional terms its unit is $\mathrm{Pa}/\sqrt{\mathrm{Hz}}$; however, pressure is normalized by $\rho_\infty a_\infty^2$ and frequency is normalized to the Strouhal number. The forcing scheme employed here does not preserve the azimuthal homogeneity of the jet. Thus, one should ideally place the reference section of the near-field microphone array at different azimuthal locations, in addition to sweeping the rotating section over the azimuth (see Appendix B). This was not done in the present experiments. However, an indirect assessment in § IV-D will demonstrate that the errors incurred are probably insignificant.

The modifications in the near pressure field amplitudes due to forcing of the heated jet at the AGR of 5.4 are presented in Figure 9(a). Apart from the forcing tones and their harmonics, there are slight differences in

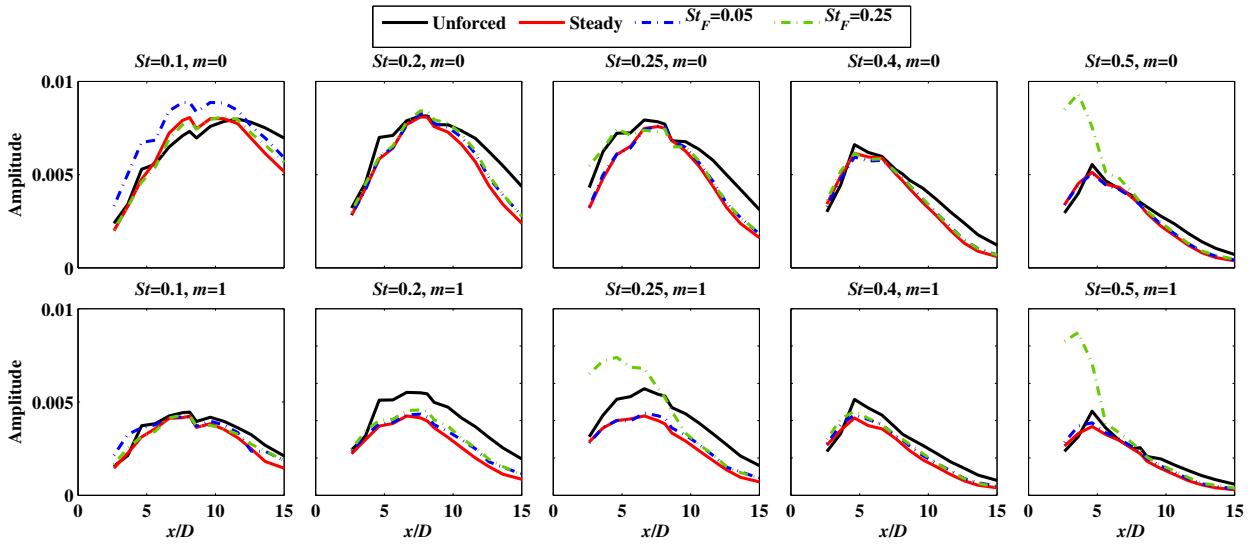

(a) Normalized modal amplitude

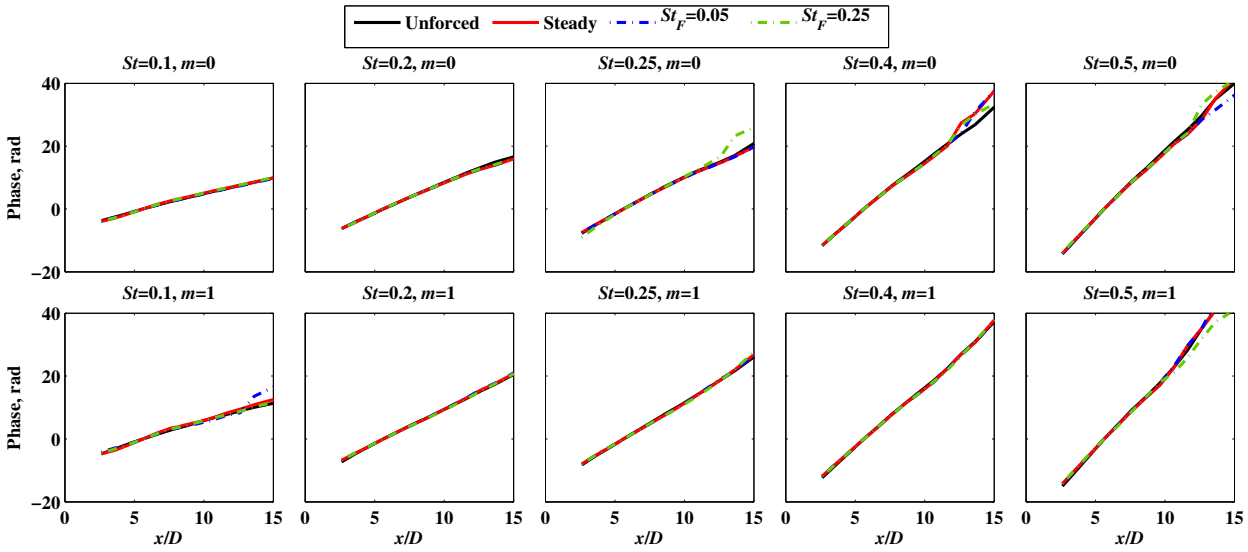

(b) Modal phase

Figure 9. Modification of near-field pressure amplitude and phase measured on the rotating cage array due to forcing of the heated jet. The actuator supply gauge pressure ratio is 5.4 in all forced cases.

the results from different forcing frequencies, the latter generally following the corresponding trends observed in the far field in figure 5. Overall, a slight amplification of the envelope is observed near the nozzle exit, especially at low frequencies, with subsequent earlier saturation and faster decay. The attenuation is greater in the $m = 1$ mode. At frequencies that are *not* harmonics of St_F, the envelopes are not distinguished by the forcing frequency. This suggests that the low-frequency dynamic content introduced by the actuators is possibly in the linear regime. At the same time, the modification of the amplitude envelopes is indicative of the changes effected in the mean flow that were observed in § IV-B. These ideas will be revisited in § V.

The pressure amplitudes peak near $x = 6D$ for most modes, so that this particular microphone location is used as the reference in computing the phase evolution along the array from the cross spectra. The microphones are sparsely spaced beyond $x = 14D$, and the computed phases therefore suffer from aliasing from this point on downstream. The streamwise development of the phase in several representative Fourier modes is depicted in figure 9(b). The increase in phase velocity associated with increasing frequencies is evident. Of particular importance for the present work is the complete lack of distinction between the results

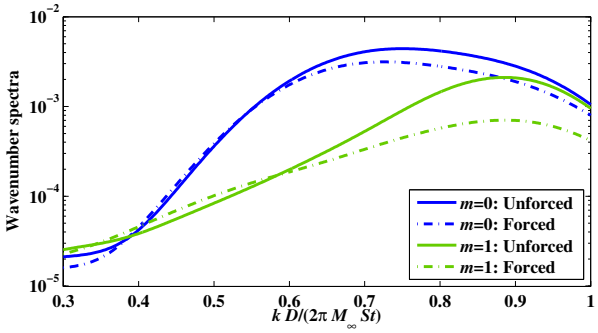

Figure 10. Streamwise wavenumber spectra at $St = 0.2$ showing the effect of steady blowing at 3.2% mass flow on the heated jet.

from different forcing conditions compared to the unforced case. This implies that the cause of any changes in the far-field acoustics due to forcing must be solely sought in the fluctuation amplitude envelopes.

The streamwise wavenumber spectrum of the near-field pressure is of particular interest for acoustics; its computation is detailed in Appendix B. If the rotating cage array were a cylindrical shell in the linear pressure field, then the streamwise wavenumber spectrum measured on it could be directly used to predict the acoustic field by solving a boundary-value Helmholtz equation.[20] For the present conical configuration, Reba et al.[6] described a more complicated calculation for accurate predictions, and this is pursued in § IV-D. However, given that the half-angle of the cone is only 7°, the wavenumber spectrum measured on it is still important for an approximate physical understanding.

The wavenumber spectra at $St = 0.2$ and modes $m = 0$ and 1 for the unforced heated jet are presented in figure 10. Just for the purpose of discussing this figure, the rotating cage will be approximated as cylindrical. Balakumar[20] provides a detailed explanation of the following arguments. The fluctuations in a given St-mode will radiate to the far field if their streamwise wavenumber k is in the range: $-1 \leq kD/(2\pi M_\infty St) \leq 1$, where M_∞ is the acoustic Mach number at the jet exit. Since the jet under consideration is convectively supersonic, the wavenumber peak is in the radiating range for both the azimuthal modes depicted. The higher wavenumbers dominate at the aft angles. Thus, the $m = 1$ mode is expected to peak further aft of the $m = 0$ mode. Their relative amplitudes are anticipated from figure 8. Furthermore, the $m = 0$ mode is more efficient at radiating noise than the $m = 1$ mode,[21] which explains the dominance of the former in the far field observed later.

The effect of steady blowing on the wavenumber spectra is a significant suppression near the peak with nominal amplification at lower wavenumbers. This modification was also anticipated from figure 9, but is especially clear and meaningful here. This explains the observation in § IV-A that the forcing selectively suppresses aft angle noise, with some amplification toward sideline angles. Moreover, the suppression in $m = 1$ mode should be greater than that in the axisymmetric mode, and this indeed conforms with further analysis below.

D. The azimuthally-decomposed acoustic mid field

The azimuthal structure of the acoustic field has been previously investigated in depth for unforced subsonic jets.[21] The study demonstrated the dominance of the axisymmetric mode of acoustic radiation to aft angles, and linked this to the enhanced acoustic efficiency of the corresponding fluctuations in the near field. It will be recalled that the mid-field acoustic array in the present experiments is at a polar angle of 159° measured from the upstream jet axis. The SPL recorded on this array is decomposed into its azimuthal Fourier modes, and the results are shown for the heated jet in figure 11. The dominance of the $m = 0$ mode is apparent in the unforced case, as expected from the discussion in § IV-C. In the same figure are also plotted the modal SPLs for the case of steady blowing at 3.2% mass flow. The significant suppression of all azimuthal modes is evident. Moreover, the level of suppression in different Fourier modes correlates well with those observed in the hydrodynamic near field in figures 9(a) and 10.

The far-field acoustic measurements are performed on a linear array so that direct azimuthal decomposition of the acoustic field is lacking over the polar arc. An alternative technique was proposed by Reba et al.,[6]

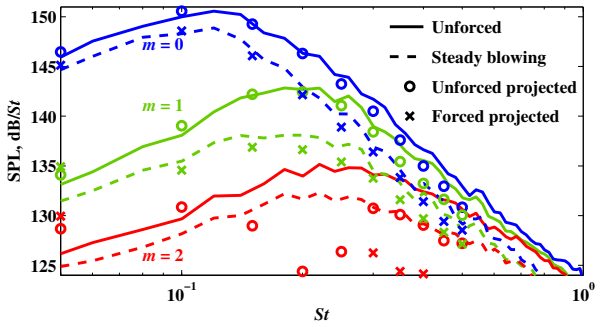

Figure 11. Azimuthal modal spectra on mid-field array in heated jet, steady blowing being at 3.2% mass flow.

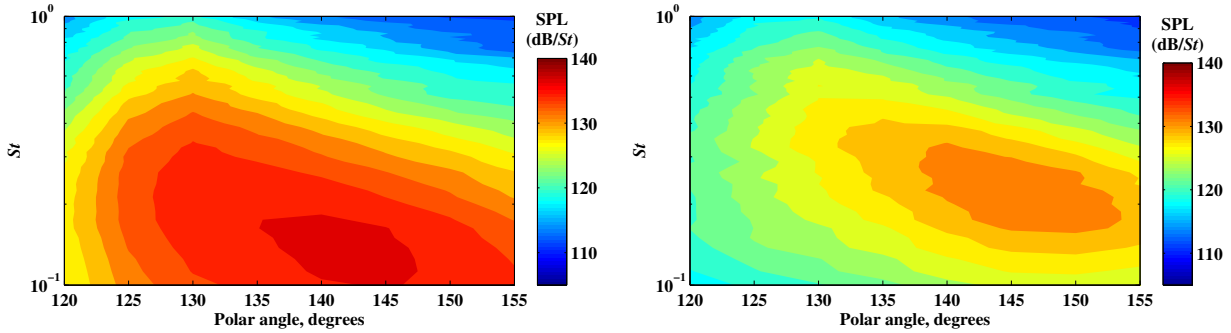

(a) Azimuthal mode $m = 0$ (b) Azimuthal mode $m = 1$

Figure 12. Azimuthal decomposition of spectral directivity in the unforced heated jet.

and this is validated here using the azimuthally decomposed mid-field array measurements. The near-field rotating cage array is designed such that it is situated in the linear pressure field.[17] Then, the pressure cross spectrum measured on this array can be used as a boundary condition in solving a homogenous Helmholtz equation for the acoustic radiation outside the array. An intermediate step was included by Reba et al.,[6] wherein the measured cross spectrum was modeled with an assumed functional form. This is particularly useful when the near-field array is so limited in its streamwise extent that it fails to capture a significant portion of the hydrodynamic energy. However, this additional complication is profitably avoided here since the present near-field array is extended further downstream than the one used by Reba et al.[6]

The results from this projection technique are compared with the direct measurements in figure 11. The agreement is very good in the energetic range of Fourier modes, both in the unforced and forced cases. Although not shown, similar matches were observed in other forcing cases too. The higher frequencies display some discrepancies. These are associated with shorter wavelengths which are beyond the resolution of the near-field array. The projection technique is not expected to perform well for much lower frequencies than those depicted, since the near field array will be unable to capture their peaks, which occur further downstream. It was discussed in § IV-C that an erroneous assumption of azimuthal homogeneity is made in computing the azimuthal Fourier decomposition of the near-field pressure in forced jets using the rotating cage array. (Note that this assumption is *not* made in decomposing the mid-field acoustic measurements.) However, the good agreement observed here in the $m = 0$ mode and the reasonable match in the $m = 1$ mode indicate that the error incurred for these dominant modes is not significant, at least in terms of their acoustic effect. The comparison for the $m = 2$ mode is very poor, possibly owing to uncertainties in measuring this higher-order low-energy azimuthal mode. Since the energy in the $m = 2$ mode is significantly lower compared to the $m = 0$ and $m = 1$ modes, the subsequent discussion omits the $m = 2$ mode.

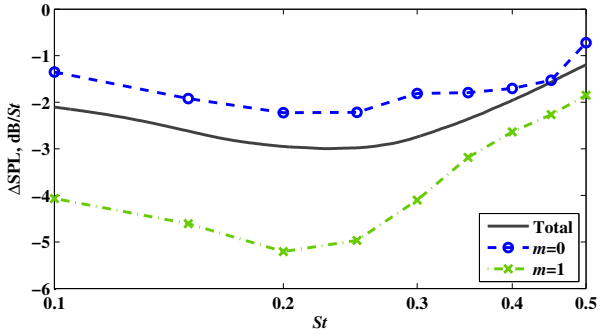

Figure 13. Effect of steady blowing at 3.2% mass flow applied to the heated jet on different azimuthal modes of the far-field spectra at the 150° polar angle.

E. Further analysis of the acoustic far field

The technique described in § IV-D for projecting the near-field pressure measurements to the far field is used to obtain the azimuthally-decomposed spectral directivities for the heated jet in figure 12. The range of polar angles is restricted since fluctuations of higher frequencies that are important for sideline propagation are poorly resolved on the near-field array. The reasons for restricting the frequency axis have been explained in § IV-D. The trends in relative strengths of the $m = 0$ and 1 modes over the range of frequencies that were observed in figure 11 carry over to all the polar angles depicted here. Namely, the axisymmetric mode is louder than the first helical mode at all frequencies, and the latter peaks at higher frequencies. In terms of directivity, figure 12 indicates that the $m = 1$ mode peaks further aft of the $m = 0$ mode. This result was anticipated from the streamwise wavenumber analysis of the near-field pressure in § IV-C. Similar characteristics were noticeable in the isothermal jet also.

Although not shown here, a further validation was pursued for the acoustic projection technique. The contributions of the $m = 0$, 1 and -1 modes were added to obtain the usual azimuthally-averaged SPL spectra, the last two modes having the same energy in the non-swirling jets considered. The result agreed well with the contours in figure 4. This also attests to the relative unimportance of azimuthal modes higher than the first helical.

The azimuthal modal decomposition of the noise benefit is analyzed for steady blowing at 3.2% mass flow on the heated jet in figure 13. The 'total' benefit curve is reproduced from figure 5(c). The azimuthal modal decomposition is obtained by projecting the respective modes from the near-field microphone array, as described in § IV-D. The frequency axis is restricted to the range where this projection technique is trusted.

Although the energies in the different azimuthal modes add up to the total, the ΔdB's do not add up since they refer to a ratio. Thus, the total noise benefit is somewhere in between the benefits in the different azimuthal modes. As anticipated from the observations in the near field and mid field, the suppression of the $m = 1$ mode is greater than that of the $m = 0$ mode for this forcing condition. However, the total curve is skewed towards the latter since the axisymmetric mode is significantly louder in the unforced condition.

An asymptotic analysis was presented by Balakumar[20] for the Helmholtz equation governing acoustic radiation from the near-field pressure. It showed that the streamwise wavenumber k in frequency mode St of the near-field pressure that contributes most to a far-field observer polar angle φ (measured from the upstream axis) is given by $kD = 2\pi M_\infty St \cos(180° - \varphi)$. The wavenumber spectrum for $St = 0.2$ was presented in figure 10, so that the spectral amplitude suppression at the dominant wavenumber for $\varphi = 150°$ can be read off. In ΔdB terms, these values are -1.8 and -4.8 for $m = 0$ and $m = 1$, respectively, which agree quite well with the observed suppression in figure 13. As mentioned in Appendix B, an explanation for minor discrepancies can be found in the underlying assumption of a cylindrical Kirchhoff surface in the asymptotic analysis, whereas the actual configuration is conical in the experiments here.

Reba et al.[22] observed very similar effects of chevrons on the isothermal Mach 1.5 jet investigated here. In particular, they found similar levels of reduction in the near and far field, in both the magnitude and shape of the spectra. Moreover, a similar reduction in the growth rate of wavepackets was demonstrated. All these support the potential of fluidic injection as a deployable alternative (or a selective augmenter) of chevrons on supersonic jets for noise mitigation, as documented by Alkislar et al.[5] for a subsonic case.

V. Modeling acoustically-dominant wavepackets

It will be recalled from § I that wavepackets are the coherent wave-like fluctuations observed in turbulent jets with correlation length scales of several jet diameters. Their convective dynamics have been associated with the dominant aft-angle mixing noise in jets.[6,7] The present research builds on a successful experimental, modeling, and computational effort aimed at developing a predictive theory for the dynamics of wavepackets in unforced supersonic jets.[10,22,23] The reduced-order model predicts the streamwise development of wavepackets as the growth, saturation, and decay of the linear instability modes of the turbulent mean flow. These instability modes, in turn, are calculated from the theory of parabolized stability equations (PSE), which is a generalization of locally-parallel stability theory to mildly non-parallel mean flows.[9,24] The only input to the linear PSE model is the empirical mean flow field (from experiments or numerical simulations), which, it must be remarked, implicitly incorporates a significant portion of the nonlinearities in the turbulent flow. We make advances with this approach in explaining the observations in the forced supersonic jets in the present work; the detailed theory can be found in our previous publications.[9,10]

A. Modeling wavepackets in the unforced jet

Wavepackets in turbulent jets are most readily observable in the irrotational pressure field just outside the shear layer. This was the motivation behind the design of the near-field microphone array employed in this work. The streamwise evolution of amplitude and phase measured for various acoustically-significant $St-m$ Fourier modes in the unforced heated jet are reproduced in figure 14 from figure 9.

Although these pressure fluctuations have significantly longer correlation length scales compared with the underlying turbulent velocity field in the shear layer, they still include some incoherent components. Gudmundsson and Colonius[9] demonstrated that proper orthogonal decomposition (POD)[25] is an effective filtering tool for extracting the dominant coherent wavepacket from the above pressure signal. The first POD mode (shown in figure 14) is the eigen-function associated with the leading-order eigenvalue of the cross-spectral density tensor defined in Appendix B. In general, the first POD mode is seen to capture the saturation region of the pressure amplitude envelope, but decays faster on either side, which implies the presence of incoherence in these regions. The phase evolution diagrams are unable to distinguish between the unfiltered and filtered data.

The linear PSE predictions of the wavepacket amplitude and phase are also presented in figure 14. The input mean flow field was described in § IV-B. The linear PSE system is homogenous, and hence it neither depends on nor predicts the absolute amplitude of the solution. Thus, the amplitude envelopes of the PSE solution for each Fourier mode is scaled herein to best fit the corresponding microphone array data.[9] The amplitude evolution predicted for the wavepackets agree reasonably well with the first POD modes for $St \geq 0.3$. The PSE assumption of slow streamwise variation of the mean flow relative to the wavepacket wavelength is violated at lower frequencies, thereby degrading those predictions.[9] The phase evolution of the instability modes are predicted very well by the reduced-order model.

The above results indicate that the acoustically-dominant wavepackets in the turbulent supersonic jet are a manifestation of *linear* instability modes of the turbulent mean flow. Similar observations were made in subsonic jets,[9,11] as well as from a large-eddy simulation database of the present experimental conditions.[10,23]

B. Modeling wavepackets in a jet forced by steady blowing

Alkislar et al.[5] have documented the similarities between chevrons and microjets in terms of the mean flow and acoustic spectral changes. A locally-parallel stability analysis of a chevroned jet was performed by Gudmundsson,[26] who linked the modifications in the mean flow to the reduced growth rate of wavepackets, thereby providing an explanation for the observed noise reduction. An analogous modeling of the effect of steady blowing in the current experiments requires greater resolution of the azimuthal variations in the mean flow than is available at present. Instead, in the preliminary modeling attempt reported here, two different *axisymmetric* mean flow fields are evaluated in conjunction with the linear PSE method. Although this approach is certain to introduce modeling errors, the results have sufficient qualitative agreement with the experiments to be of value for the analysis.

Figure 15 presents the first POD mode of the near-field pressure calculated from the case of steady blowing at 3.2% mass flow on the heated jet. For comparison, the first POD mode of the unforced pressure signal, as well as the corresponding fitted PSE solution, are reproduced from figure 14(a). As anticipated

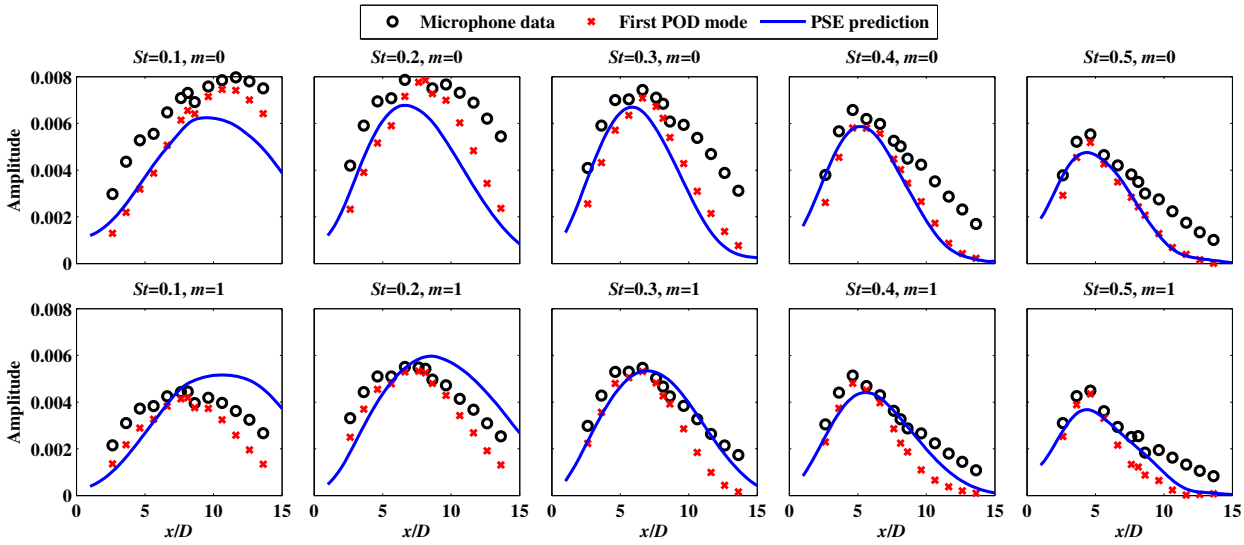

(a) Amplitude

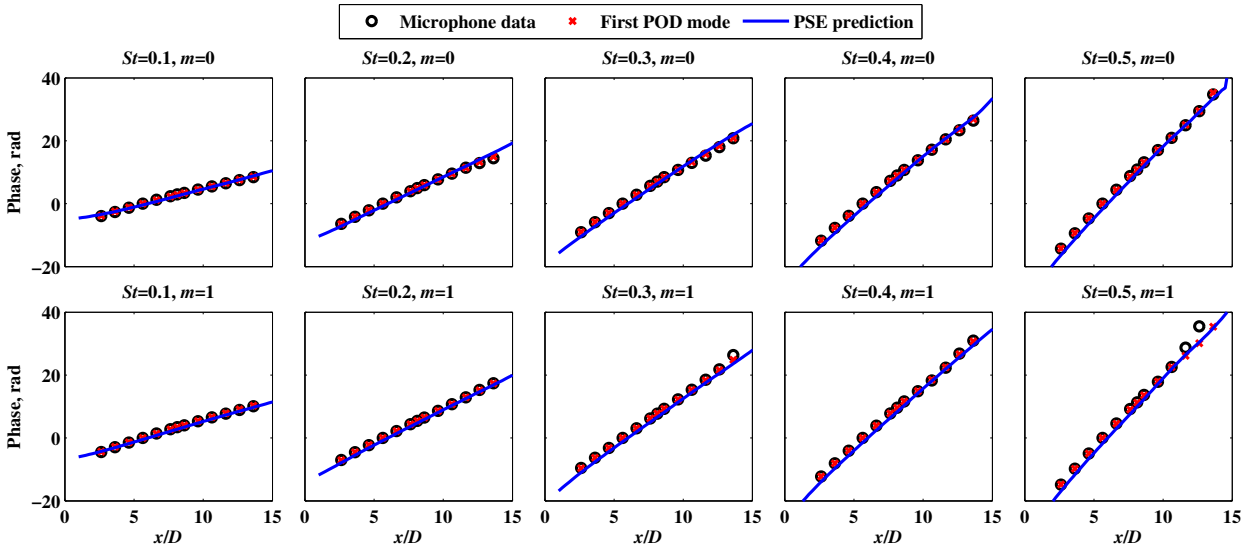

(b) Phase

Figure 14. Amplitude and phase of pressure fluctuations measured on the near-field rotating array and their first POD modes, compared with scaled linear PSE predictions for the unforced heated jet.

from the unfiltered microphone signals in figure 9(a), the coherent amplitude envelopes also display modest suppression for the axisymmetric mode, and somewhat more significant attenuation for the first helical mode.

The first mean flow field to be evaluated with PSE is the one recorded in the azimuthal plane of the injection ports, and depicted in figure 7(b) as the 'Forced: 0 deg' case. This choice was guided by the fact that the fixed reference array in the near field is aligned with an injection port (see figure 1(a)). Thus, the azimuthal Fourier modes of pressure estimated with this configuration may be thought to be biased toward those associated with the above mean flow (see § IV-C and Appendix B for further discussions). The resulting PSE modes are presented in figure 15, scaled so that the amplitudes at the initial axial station match those computed for the unforced jet. The rationale for this is that the disturbance spectrum near the nozzle exit is expected to remain unchanged even with forcing, and only the downstream evolution of the instabilities should be affected. The PSE model is predicting the correct effect, viz. suppression. The reduction in initial growth rate of the instability modes is qualitatively explained by the thickening of the shear layer caused by the actuation, as clearly observed in figure 7(b). However, the magnitude of the

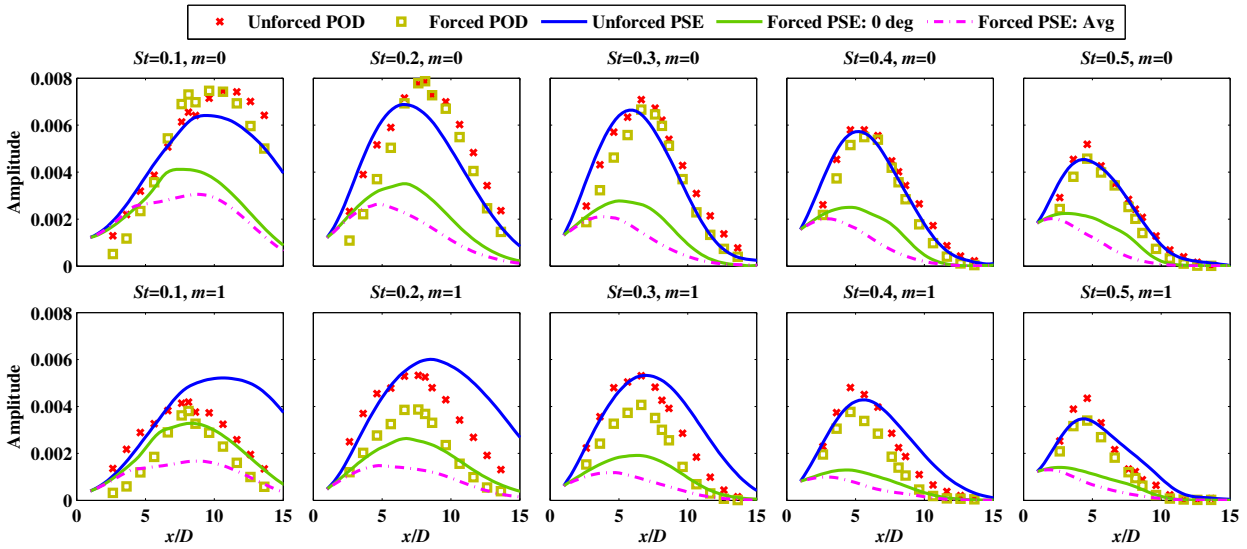

Figure 15. PSE model prediction of the modification of wavepacket amplitudes on the near-field rotating array due to steady blowing at 3.2% mass flow applied to the heated jet.

suppression is substantially over-predicted. Moreover, the predicted levels of attenuation are similar in the $m = 0$ and 1 modes, whereas the observed suppression in the latter significantly outweighs that in the former.

Prior to further discussion of the above result, it is instructive to also consider the PSE result using the second mean flow field. This is calculated as an average of the mean flow profiles sampled at the two different azimuthal planes depicted in figure 7(b). This then represents the effective axisymmetric mean flow, neglecting the corrugations superposed on it. The resultant PSE modes presented in figure 15 display even greater suppression compared to the aforementioned solution. It was shown in figure 7(b) that the '0 deg' mean flow profile used in the previous calculation has a thinner shear layer compared to the '45 deg' profile that is added to obtain the average mean flow in the second solution here. This accounts for the further decrease in the growth rate of the instability modes observed in the second case.

There are several possible reasons for the over-prediction of the levels of suppression. The actual mean flow has an additional shear in the cross-stream plane that is neglected. This shear can enhance the growth rates of the instabilities captured here, or, more likely, can yield additional instability modes. This effect was investigated for chevroned jets by Gudmundsson.[26]

A related effect that is also neglected in the present model is the coupling of different azimuthal modes through the dominant modes of the mean flow.[26] With four injection ports around the periphery, the mean flow field is composed of azimuthal modes $0, \pm 4, \pm 8$, etc. As a result, the $m = 0, \pm 4, \pm 8, \ldots$ modes form a coupled mode set. As another example, the $m = 1, -3, 5, -7, 9, \ldots$ modes constitute another coupled set. Though not reported here in further detail, an attempt was made to evaluate the relevance of these couplings using nonlinear PSE. However, no significant effect was found in the fundamental modes of the above sets. This idea will be pursued further in subsequent research.

The final possible reason for the discrepancy is concerned with the experimental data itself. As discussed in § IV-C and Appendix B, the azimuthal Fourier decomposition of the near-field pressure has some associated errors since the reference array was fixed at a single azimuthal angle. The far-field acoustic prediction from these measurements appear to be unaffected by this inaccuracy (see figure 11). However, it must be recalled that the latter was investigated on a logarithmic scale whereas the present examination uses a linear scale. Thus, there is a possibility that the true azimuthal modes of the near-field pressure (if they were measured) would have been better approximated by PSE. Further experimentats are required to address this issue.

In summary, the effect of steady blowing in suppressing the wavepacket amplitudes (and hence the far-field noise) is qualitatively explained by the reduced-order model. It demonstrates that the thickening of the shear layer near the nozzle is responsible for reduced growth rate of the instability modes that dictate the downstream evolution of the acoustically-dominant wavepackets. However, further refinement of the model is necessary to arrive at a firmer conclusion.

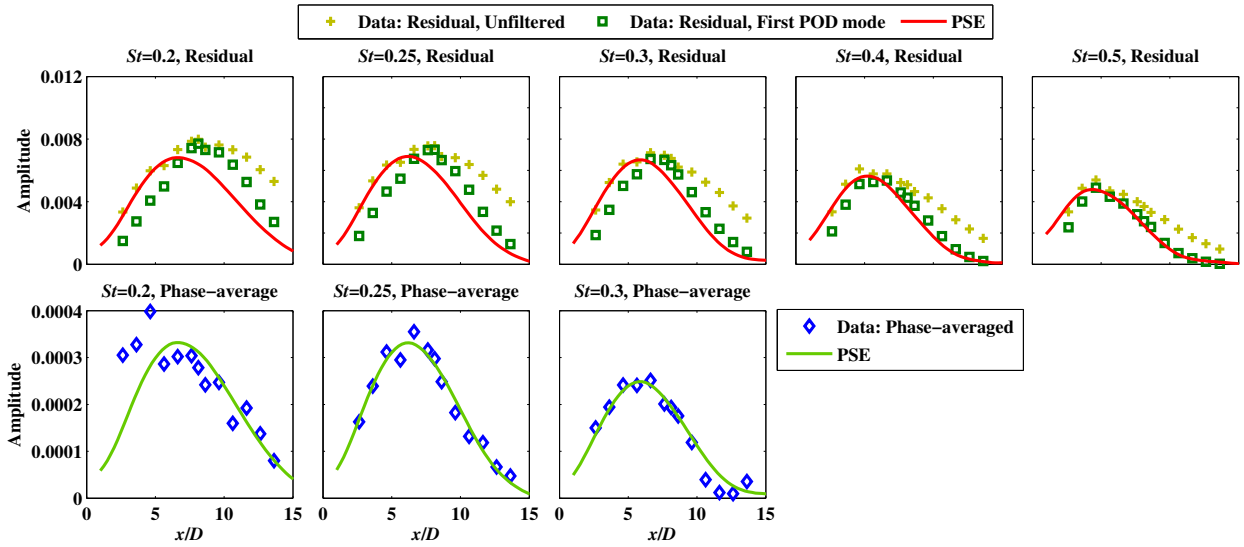

(a) Axisymmetric mode forcing at $St_F = 0.05$

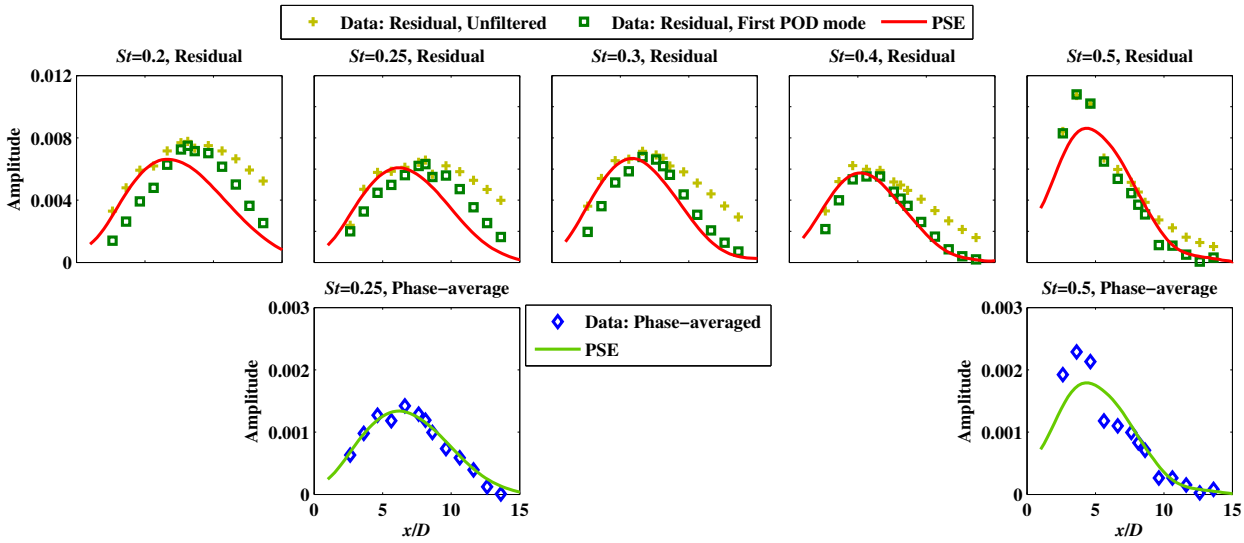

(b) Axisymmetric mode forcing at $St_F = 0.25$

Figure 16. PSE prediction of phase-averaged and residual (i.e. uncorrelated) components of near-field pressure fluctuations at the $m = 0$ mode in the heated jet harmonically-forced at an actuation supply gauge pressure ratio of 2.7.

C. Modeling wavepackets in harmonically-forced jets

The actuator characterization in § III has demonstrated that the harmonic content introduced by air injection is almost independent of the valve plenum pressure. On the other hand, the mass flow rate delivered is a function of the plenum pressure, but independent of the forcing frequency. Furthermore, comparisons of near-field and far-field pressure have demonstrated that the trends in amplitude suppression are similar for steady and harmonic forcing schemes (with the exception of the appearance of narrow-band tones in the latter) if the same AGR is employed. Then, the results with steady blowing shown in figure 6(a) imply that harmonic forcing of the heated jet at AGR of 2.7 (MFP = 2.0%) should not significantly modify the broadband turbulence spectrum from the unforced condition, although it introduces substantial harmonic content into the flow. The discussion in § V-B has linked changes in broadband turbulence spectrum with the modification of the mean flow field. Thus, the mean flow field for the unforced heated jet is used here as the base flow in modeling the effect of harmonic forcing at AGR of 2.7.

Triple decomposition[27] is a convenient tool for separating the harmonic response of turbulent flows from the changes effected by harmonic forcing to the broadband turbulence. The pressure signals recorded on the near-field microphone array are decomposed into the mean (which is the ambient pressure for the free jets under consideration), the phase-averaged portion that is correlated to the actuation (using the encoder signal from the spinning valve motor), and the residual (i.e., the uncorrelated part).

These components are shown in figure 16 for two forcing frequencies. The phase-averaged portion is further decomposed (by discrete time Fourier transform) into the fundamental and higher harmonics.[28] The design of the actuation system results in the excitation of several harmonics of the fundamental forcing frequency (see also figure 5). Furthermore, as discussed in § V-A, the correlated wavepacket in the residual component is extracted as its first POD mode. The forcing is axisymmetric in the sense that all four injection ports pulse in synchrony. So, only the $m = 0$ mode of the pressure is studied here. The restriction of the modal frequencies to $0.2 \leq St \leq 0.5$ is guided by the success of linear PSE in this range (see § V-A).

The phase-averaged component is modeled by linear PSE with good accuracy for both the forcing frequencies $St_F = 0.05$ and 0.25. There are some discrepancies near the nozzle, which may be due to direct propagation of injected pressure pulses to these microphones. It must be remarked that the depicted harmonics for the $St_F = 0.05$ forcing have very little energy, although these are more substantial with $St_F = 0.25$. However, the agreement with linear PSE is reasonable for both cases. This implies that the harmonic content introduced by the spinning valve actuator is evolving downstream through the corresponding linear instability mode of the underlying turbulent mean flow.

The residual component of the wavepacket which represents the broadband part of the turbulence spectrum is also modeled reasonably accurately by the linear PSE solutions, albeit with a different scaling (as discussed in § V-A). In fact, the degree of match is no different than in the unforced jet. Furthermore, the amplitude of the residual portion does not change when the two different forcing frequencies are used, with one exception that is discussed below. This is in keeping with the observations in figure 9(a), which were for the total pressure fluctuations (not just the residual part) with the higher mass flow rate of injection. The implication is that the broadband turbulence spectrum is not affected by the harmonic content injected, and the corresponding wavepackets continue to be well-predicted by linear instability theory.

The exception is noted in the case of the $St = 0.5$ mode of the residual component for forcing at $St_F = 0.25$. In this mode, the wavepacket amplitude is significantly higher than that in the unforced jet. At the high rotation speed (5000 rpm), the valve may have intermittent mechanical vibrations due to minor rotor imbalance. Such intermittency may explain why this signature is rejected by the phase-averaging, but manifests in an amplified residual component.

The foregoing analysis leads to the tentative conclusion that, for the unsteady actuation schemes considered in this research, wavepackets induced by the harmonic component of the actuation are linearly superposed on those produced by broadband turbulence without significant interaction. Thus, the harmonic content adds tones to the far-field noise that are counterproductive as far as noise reduction is concerned. All the noise benefit appears to derive from the modifications in the mean flow effected by the steady component of the injection.

VI. Conclusions

A comprehensive physics-based approach is being undertaken to search for solutions to the supersonic jet noise reduction problem. The theoretical aspect of the research involves a reduced-order modeling approach based on parabolized stability equations (PSE). This is intended to be an efficient technique for evaluating the effect of various forcing strategies on the far-field acoustics. The experiments evaluate a novel spinning-valve actuator for noise-mitigation. Results in isothermal and heated Mach 1.5 jets indicate $\sim$ 2 dB of OASPL benefit in the peak aft angles, and 2 to 3 dB of benefit near peak frequencies of the spectrum. For the same injection plenum pressure, steady blowing yields more noise benefit than the unsteady actuation schemes evaluated. However, this may be explained by the slight decrease in injection velocity incurred in going from steady to unsteady operation.

The experiments are particularly remarkable for the detailed diagnostic techniques that are brought to bear on the problem. Analysis of the resulting data allows us to track the cause of far-field noise benefit to the near-field hydrodynamic pressure. It is thus found that the noise suppression is a consequence of attenuation of the amplitude of wavepackets, with no discernible change in their phase speeds.

The database of forcing conditions thus generated is also intended for validating the PSE model that

links observed changes in the turbulent mean flow field to the wavepackets. Results presented here indicate reasonable match between PSE prediction and experimental observation of the streamwise evolution of the acoustically-important wavepackets in the unforced jet. The effect of steady blowing is to suppress the wavepacket amplitude through thickening of the shear layer near the nozzle. The preliminary model for this has several additional assumptions that weaken the quantitative agreement, but the trend is captured qualitatively. Finally, the model indicates that, in the case of unsteady forcing, the harmonic content introduced into the flow develops independently through the same linear instability mechanism as the residual uncorrelated fluctuations. Thus, it appears that the unsteady actuation schemes pursued here are unable to directly affect the broadband turbulence, and hence the far-field noise. These schemes are having the same indirect effect on the noise field as an equivalent steady blowing, by modification of the mean flow field mentioned above. However, by adding tones to the noise spectra, they serve to degrade the noise benefit.

Recently, Cuppoletti et al.[2] reported that, compared to steady blowing, very low frequencies of pulsing can produce higher noise benefit for the same injection mass flow rate, which would indicate a possible advantage of unsteady actuation. In the present experiments, the mass flow rate for unsteady forcing was not measured. However, the observed modification of injection velocity with pulsation does not discard this possibility.

The research is being extended in several directions at present. Further diagnostics, like time-resolved shadowgraphy, will be used to detect the instantaneous changes in the flow field caused by unsteady actuation. A variety of other actuation strategies are also being evaluated in experiments. In particular, the next phase of the study may be directed at optimizing the spinning valve dynamics to provide a distinct steady and unsteady forcing, now that procedures have been defined for establishing the cause-effect link between injection, the near-field instability/wavepacket evolution, and the far-field sound.

Appendix

A. Composing smooth mean flow field from sparse point measurements

The mean streamwise velocity and temperature fields are estimated from sparse point measurements. Several empirical functions are fitted to the data to obtain a smooth field. The fits for the unforced and forced jets are in good agreement with the data in figure 7. The mean centerline streamwise velocity is fitted as follows

$$\overline{U}_x\left(x, r=0\right) = \begin{cases} U_j, & 0 \le x \le x_u \\ U_j - R_u + \sqrt{R_u^2 - \left(x - x_u\right)^2}, & x_u \le x \le x_U \\ u_n/\left(x + u_d\right), & x_U \le x. \end{cases} \tag{1}$$

The downstream decay function is commonly used for self-preserving jets,[29] whereas the intermediate arc portion is ad hoc. The parameters U_j, R_u, u_n and u_d are determined by nonlinear least-squares fit to the experimental data. The remaining parameters, viz. x_u and x_U, are determined by requiring that the arc and decay portions be tangential at x_U.

The assumed functional form of the mean centerline temperature is

$$\overline{T}\left(x, r=0\right) = \begin{cases} T_j, & 0 \le x \le x_t \\ T_j + t_3\left(x - x_t\right)^3 + t_2\left(x - x_t\right)^2, & x_t \le x \le x_T \\ t_n \Big/ \left(x + t_d\right)^2 + 1, & x \ge x_T. \end{cases} \tag{2}$$

The form of the decay function is a consequence of the quadratic dependence of the temperature on the velocity (as in the Crocco-Busemann relation), which in turn is assumed to decay linearly above. The intermediate cubic spline portion is ad hoc. The parameters T_j, t_n, t_d, x_t and x_T are determined by nonlinear least-squares fit to the data. The remaining parameters, viz. t_2 and t_3 are calculated from the geometric constraint of tangentiality of the middle cubic spline with the downstream quadratic decay section at x_T.

The radial profile of the mean streamwise velocity is fitted with a Gaussian function[30]

$$\overline{U}_x\left(x, r\right) = \overline{U}_x\left(x, r=0\right) \exp\left\{ -\ln(2) \left(\frac{|r| - h(x)}{b(x)} \right)^2 \right\}. \tag{3}$$

The half-width of the annular shear layer $b(x)$ is interpolated by a cubic spline in between measurement cross-sections. Within the potential core region ($0 \leq x \leq x_u$), the inner edge of the shear layer $h(x)$ is computed to maintain constant momentum flux, the constant value being the median value determined from fits at the measurement cross-sections. In the self-similar region $h(x) = 0$, and the transition is effected with a cubic spline.

The radial profile of the mean temperature field is determined from the Crocco-Busemann formula, with the constants calculated separately at each axial station from the fitted mean centerline temperature and streamwise velocity described above. Finally, the mean radial velocity is computed from the continuity equation. For the forced jets, azimuthal inhomogeneity results in non-zero azimuthal velocity. In the absence of experimental data, this is set to zero as in the case of the unforced round jet.

B. Post-processing of pressure measurements

The pressure is measured on the rotating cage array in the near irrotational field; the location on it is indicated by the x coordinate. Prior to the temporal transform, the time-series of pressure is divided into (possibly overlapping) windows indexed by l, as in the Welch spectrogram method. This pressure signal is denoted by $p^{[l]}(x, \theta, t_j)$, where θ is the azimuthal angle, and t_j is the discretely-sampled time with index j. Let the sampling frequency by f_s and each time window contain N samples. The following short-time discrete Fourier transform is then computed:

$$\check{p}^{[l]}(x, \theta, f_n) := \frac{\sqrt{2 - \delta_{f,0}}}{\sqrt{f_0} N} \sum_{j=0}^{N-1} w_j p^{[l]}(x, \theta, t) \exp(2\pi \mathrm{i} n j / N), \quad f_n = n f_0, \quad f_0 = f_s / N. \tag{4}$$

Here, f refers to the spectral frequency, and it is obtained at discrete values. The particular normalization makes the spectral amplitude independent of the sampling and windowing characteristics. Moreover, w_j denotes to the weight assigned to the jth sample by the Hanning window function used here.

The next step is the computation of the azimuthal cross-correlation

$$R(x_1, x_2, \vartheta, f) := E\left[\check{p}^{[l]}(x_1, \theta + \vartheta, f_n) \left\{\check{p}^{[l]}(x_2, \theta, f_n)\right\}^{\mathrm{H}}\right]_{l,\theta}. \tag{5}$$

The expectation operator is denoted by $E(\cdot)$, and the azimuthal homogeneity is exploited to evaluate the expectation over the different azimuthal locations of the reference microphone, if available. The expectation is also performed over the different segments of the time-series. Since unforced round jets are statistically axisymmetric, the azimuthal averaging is not essential for them. However, most forcing schemes, including the one employed here, do not preserve the axisymmetry, so that azimuthal averaging becomes essential for correct evaluation.

The azimuthal-modal cross spectral density is then obtained as

$$CSD(x_1, x_2, m, f) := \frac{1}{2\pi} \int_{-\pi}^{\pi} R(x_1, x_2, \vartheta, f) \exp(-\mathrm{i} m \vartheta) \, \mathrm{d}\vartheta, \tag{6}$$

where m refers to the azimuthal mode. The power spectral density is the diagonal of the cross spectral tensor calculated above.

The conical half-angle of the rotating cage array is only 7°, so that an approximate streamwise wavenumber spectrum may be calculated from measurements made on it:

$$S(k, m, f) \equiv \int_{-\infty}^{\infty} \int_{-\infty}^{\infty} CSD(x_1, x_2, m, f) \exp\{\mathrm{i} k (x_1 - x_2)\} \, \mathrm{d}x_1 \mathrm{d}x_2. \tag{7}$$

The streamwise wavenumber is denoted by k. The integrals are truncated to the available extent of the array, but this is adequate since the pressure signatures have approximate compact support within the array for most modes of interest.

Acknowledgments

The authors gratefully acknowledge support from the Office of Naval Research under contract N0014-11-1-0753 with Dr. Brenda Henderson as technical monitor, and from NAVAIR under STTR contract N68335-11-C-0026 with Dr. John Spyropoulos as technical monitor.

References

[1]Henderson, B., "Fifty years of fluidic injection for jet noise reduction," *International Journal of Aeroacoustics*, Vol. 9, No. 1-2, 2010, pp. 91–122.

[2]Cuppoletti, D., Gutmark, E., Hafsteinsson, H., Eriksson, L.-E., and Prisell, E., "A comprehensive investigation of pulsed fluidic injection for active control of supersonic jet noise," *51st AIAA Aerospace Sciences Meeting, AIAA Paper 2013-0009*, 2013.

[3]Kuo, C.-W., Morris, P. J., and McLaughlin, D. K., "Noise Reduction in Supersonic Jets by Nozzle Fluidic Inserts," *18th AIAA/CEAS Aeroacoustics Conference, AIAA Paper 2012-2210*, 2012.

[4]Samimy, M., Kim, J.-H., Kearney-Fischer, M., and Sinha, A., "High-Speed and High Reynolds Number Jet Control Using Localized Arc Filament Plasma Actuators," *Journal of Propulsion and Power*, Vol. 28, No. 2, 2012, pp. 269–280.

[5]Alkislar, M. B., Krothapalli, A., and Butler, G. W., "The effect of streamwise vortices on the aeroacoustics of a Mach 0.9 jet," *Journal of Fluid Mechanics*, Vol. 578, 2007, pp. 139–169.

[6]Reba, R., Narayanan, S., and Colonius, T., "Wave-packet models for large-scale mixing noise," *International Journal of Aeroacoustics*, Vol. 9, No. 4-5, 2010, pp. 533–558.

[7]Jordan, P. and Colonius, T., "Wave Packets and Turbulent Jet Noise," *Annu. Rev. Fluid Mech.*, Vol. 45, 2013, pp. 173–195.

[8]Narayanan, S., Barooah, P., and Cohen, J. M., "Dynamics and control of an isolated jet in cross flow," *AIAA Journal*, Vol. 41, No. 12, 2003, pp. 2316–2330.

[9]Gudmundsson, K. and Colonius, T., "Instability wave models for the near-field fluctuations of turbulent jets," *Journal of Fluid Mechanics*, Vol. 689, 2011, pp. 97–128.

[10]Rodriguez, D., Sinha, A., Brès, G., and Colonius, T., "Parabolized stability equation models in turbulent supersonic jets," *18th AIAA/CEAS Aeroacoustics Conference, AIAA Paper 2012-2117*, 2012.

[11]Cavalieri, A. V. G., Rodriguez, D., Jordan, P., Colonius, T., and Gervais, Y., "Wavepackets in the velocity field of turbulent jets," *18th AIAA/CEAS Aeroacoustics Conference, AIAA Paper 2012-2115*, 2012.

[12]Schlinker, R. H., Simonich, J. C., and Reba, R., "Flight effects on supersonic jet noise from chevron nozzles," *17th AIAA/CEAS Aeroacoustics Conference, AIAA Paper 2011-2703*, 2011.

[13]Brown, C. A. and Bridges, J., "Small hot jet acoustic rig validation," Tech. rep., NASA TM-2006-214234, 2006.

[14]Barooah, P., Anderson, T. J., and Cohen, J. M., "Active Combustion Instability Control With Spinning Valve Actuators," *Proc. of ASME Turbo Expo, GT-2002-30042*, 2002.

[15]Proscia, T. W. and Cohen, J. M., "Modulation of a liquid-fuel jet in an unsteady cross-flow," *Proc. of ASME Turbo Expo, GT-2001-0048*, 2001.

[16]Narayanan, S., Barooah, P., and Cohen, J. M., "Experimental study of the coherent structure dynamics & control of an isolated jet in cross flow," *AIAA Paper 2002-0272*, 2002.

[17]Reba, R., Simonich, J. C., and Schlinker, R. H., "Measurement of Source Wave-Packets in High-Speed Jets and Connection to Far-Field Sound," *14th AIAA/CEAS Aeroacoustics Conference, AIAA Paper 2008-2891*, 2008.

[18]Fuchs, H. V. and Michel, U., "Experimental Evidence of Turbulent Source Coherence Affecting Jet Noise," *AIAA Journal*, Vol. 16, No. 9, 1978, pp. 871–872.

[19]Suzuki, T. and Colonius, T., "Instability waves in a subsonic round jet detected using a near-field phased microphone array," *Journal of Fluid Mechanics*, Vol. 565, 2006, pp. 197–226.

[20]Balakumar, P., "Prediction of supersonic jet noises," *36th AIAA Aerospace Sciences Meeting, AIAA Paper 1998-1057*, 1998.

[21]Cavalieri, A. V. G., Jordan, P., Colonius, T., and Gervais, Y., "Axisymmetric superdirectivity in subsonic jets," *Journal of Fluid Mechanics*, Vol. 704, 2012, pp. 388–420.

[22]Reba, R., Simonich, J. C., and Schlinker, R. H., "Chevron Nozzle Effects on Wavepacket Sources in a Supersonic Jet," *18th AIAA/CEAS Aeroacoustics Conference, AIAA Paper 2012-2253*, 2012.

[23]Brès, G., Nichols, J., Lele, S. K., and Ham, F. E., "Towards Best Practices for Jet Noise Predictions with Unstructured Large Eddy Simulations," *42nd AIAA Aerospace Sciences Meeting and Exhibit, AIAA Paper 2012-2965*, 2012.

[24]Herbert, T., "Parabolized stability equations," *Annu. Rev. Fluid Mech.*, Vol. 29, 1997, pp. 245–283.

[25]Lumley, J. L., "The Structure of Inhomogeneous Turbulent Flows," *Atm. Turb. and Radio Wave Prop.*, edited by A. M. Yaglom and V. I. Tatarsky, Nauka, Moscow, 1967, pp. 166–178.

[26]Gudmundsson, K., *Instability wave models of turbulent jets from round and serrated nozzles*, Ph.D. thesis, California Institute of Technology, 2010.

[27]Hussain, A. K. M. F. and Reynolds, W. C., "The mechanics of an organized wave in turbulent shear flow," *Journal of Fluid Mechanics*, Vol. 41, No. 2, 1970, pp. 241–258.

[28]Maury, R., Cavalieri, A. V. G., Jordan, P., Delville, J., and Bonnet, J.-P., "A study of the response of a round jet to pulsed fluidic actuation," *17th AIAA/CEAS Aeroacoustics Conference, AIAA Paper 2011-2750*, 2011.

[29]Hussein, H. J., Capp, S. P., and George, W. K., "Velocity measurements in a high-Reynolds-number, momentum-conserving, axisymmetric, turbulent jet," *Journal of Fluid Mechanics*, Vol. 258, 1994, pp. 31–75.

[30]Tam, C. K. W. and Burton, D. E., "Sound generated by instability waves of supersonic flows. Part 2. Axisymmetric jets," *Journal of Fluid Mechanics*, Vol. 138, 1984, pp. 273–295.